Journal of Power Sources 254 (2014) 232–240

Contents lists available at ScienceDirect

Journal of Power Sources

journal homepage: www.elsevier.com/locate/jpowsour

Comparing shut-down strategies for proton exchange membrane fuel cells

Alejandro Oyarce [a,*], Erik Zakrisson [b], Matthew Ivity [b], Carina Lagergren [a], Axel Baumann Ofstad [b], Andreas Bodén [b], Göran Lindbergh [a]

[a] Department of Chemical Engineering and Technology, Applied Electrochemistry, KTH Royal Institute of Technology, SE-10044 Stockholm, Sweden
[b] PowerCell Sweden AB, SE-418 34 Gothenburg, Sweden

HIGHLIGHTS

- Five different shut-down strategies for PEMFCs were evaluated in a single cell.
- H_2 purge of the cathode and O_2 consumption are the most effective strategies.
- The H_2 purge strategy had a total degradation rate of 23 μV cycle^{-1}.
- The present degradation rate is low, considering the use of unprotected start-ups.

ARTICLE INFO

Article history:
Received 27 August 2013
Received in revised form
28 November 2013
Accepted 10 December 2013
Available online 31 December 2013

Keywords:
System strategies
Start-up and shut-down
Carbon corrosion
Catalyst support
Proton exchange membrane fuel cell

ABSTRACT

Application of system strategies for mitigating carbon corrosion of the catalyst support in proton exchange fuel cells (PEMFCs) is a requirement for PEMFC systems, especially in the case of systems for transport application undergoing thousands of start-ups and shut-downs (SU/SD) during its lifetime. This study compares several of the most common shut-down strategies for 1100 cycles SU/SD cycles at 70 °C and 80% RH using commercially available fuel cell components. Each cycle simulates a prolonged shut-down, i.e. finishing each cycle with air filled anode and cathode. Furthermore, all start-ups are unprotected, i.e. introducing the H_2 rich gas into an air filled anode. Finally, each cycle also includes normal fuel cell operation at 0.5 A cm^{-2} using synthetic reformate/air. H_2 purge of the cathode and O_2 consumption using a load were found to be the most effective strategies. The degradation rate using the H_2 purge strategy was 23 μV cycle^{-1} at 0.86 A cm^{-2} using H_2 and air at the anode and cathode, respectively. This degradation rate may be regarded as a generally low value, especially considering that this value also includes the degradation rate caused by unprotected start-ups.

1. Introduction

Considerable attention has been focused on the degradation of the catalyst support in proton exchange membrane fuel cell (PEMFC) electrodes since the work published by Reiser et al. [1]. Under fuel starvation conditions or during start-ups and shut-downs (SU/SD), H_2 and O_2 may coexist at the anode compartment, forcing the cathode to reach high potentials and resulting in severe corrosion of the carbon support [1]. This loss of carbon significantly increases catalyst degradation rates, characterized by a decrease in electrochemically active surface area (ECSA) [2]. Carbon corrosion may also result in considerable changes to the electrode morphology e.g. thinning of the electrode [3,4], formation of cavities [5], and decreased electrode porosity, usually referred to as electrode collapse [6]. The combined effect of these physical changes results in severe degradation of the fuel cell performance, especially at high current densities where mass transport may become limited by the altered electrode morphology [6,7].

The four main strategies to avoid this problem are: *i*) to find new carbon materials as catalyst support that are able to sustain corrosion [8,9], *ii*) not to use carbon as a support for the Pt catalyst [10–12], *iii*) to add catalysts with high activity towards the oxygen evolution reaction (OER) to the Pt-based cathode [13] and/or to add catalysts with low activity towards the oxygen reduction reaction (ORR) to the Pt-based anode [14] and *iv*) to apply system strategies to minimize or avoid carbon corrosion at the cathode. Although strategies *i*–*iii* are considered by fuel cell system developers to be promising alternatives to address issues related to SU/SD, many of

* Corresponding author. Tel.: +46 763414275; fax: +46 8249366.
E-mail address: alob@kth.se (A. Oyarce).

0378-7753/$ – see front matter © 2013 Elsevier B.V. All rights reserved.
http://dx.doi.org/10.1016/j.jpowsour.2013.12.058

these alternative materials are still under development and often not commercially available. Thus, today's fuel cell system developers that are in need of low cost alternative to avoid issues related to SU/SD, usually turn to strategy *iv*.

An effective system approach to minimize the detrimental effects caused by unprotected SU/SD is to control certain fuel cell operating parameters. Cho et al. [4,15] showed that low cathode humidity and low cell temperature during SU/SD may increase the lifetime of the fuel cell. On the other hand, simply controlling these operating conditions is thought not to be sufficient to achieve required automotive lifetime targets, i.e. 5000 h of operation, including 30.000 SU/SD with less than 30 mV decay at rated power [16].

There has been a great deal of research in the area of system strategies for the mitigation of carbon corrosion during SU/SD. Yu et al. [17] have recently reviewed this area of research and reported that the most common strategies involve: *i*) minimize the residence time of the H_2/O_2 front at the anode, *ii*) completely prevent the H_2/O_2 front at the anode and *iii*) control the cathode potential. Strategies involving gas purge, such as N_2-purge of the anode [18], air-purge of the anode [19,20], exhaust gas recycling purge of the anode [21] and H_2-purge of the cathode [22,23] have been reported to be very successful. In addition, auxiliary loads, also called dummy loads, have been implemented to consume residual O_2 from the cathode [24,25] or residual H_2 from the anode [26] and have also been reported to be very successful.

The authors of this paper are aware that established fuel cell system developers, e.g. UTC, General Motors Corporation (GM), Honda, Ford, Toyota, Nissan, and Daimler have all carried out a great deal of research in this area and most certain already have a strategy in place for their particular systems. However, there is a lack of consensus on what are the most appropriate ways to start-up and shut-down a PEMFC. Future fuel cell system developers will still have to deal with this issue, carrying out their own expensive and time consuming research. In an effort to partially alleviate that burden, this study compares a few of the most common shut-down strategies.

The primary aim of the study is to find suitable shut-down procedures for PEMFC-based auxiliary power units (APUs) running on hydrogen rich gas. This however does not exclude that the investigated shut-down strategies could be applicable on other PEMFC applications. The strategies are named: *i*) *No purge*, *ii*) *Air purge*, *iii*) *H_2 consumption*, *iv*) *O_2 consumption* and *v*) *H_2 purge*. With the exception of the *No purge* shut-down, these strategies are evaluated in a single cell set-up for 1100 SU/SD, using commercially available fuel cell components. Each cycle is intended to simulate a prolonged shut-down, i.e. finishing each cycle with air filled anode and cathode. Furthermore, all start-ups are unprotected, i.e. H_2 rich gas is introduced into an air filled anode. Finally, each cycle also includes normal fuel cell operation at 0.5 A cm^{-2}, which better simulates realistic fuel cell conditions preceding a shut-down, e.g. water at the cathode and oxide-free Pt surface. It is not the aim of this paper to give a detail description about the involved mechanisms of each particular strategy. However, the effectiveness of the individual strategies to protect the cathode from degradation is discussed.

2. Experimental

2.1. Fuel cell hardware and electrochemical characterization

A fresh commercially available 50 μm membrane electrode assemblies (MEAs) (25 μm membrane) with loadings of 0.45 mg cm^{-2} Pt-alloy on the anode and 0.4 mg cm^{-2} Pt on the cathode was used in each of the shut-down strategy. The same type of gas diffusion layer (GDL), with micro porous layer (MPL) (Sigracet®), was used at both anode and cathode. Fig. 1 illustrates the experimental set-up used to carry out the study. The in-house fuel cell has previously been described in detailed by Ihonen et al. [27,28]. The fuel cell had cylindrical current collectors made of graphite KC-673 (Svenska Tanso AB), having an active area and flow field of 7 cm^2. The design of the flow field consisted of a single spiral flow channel with width, height and land of 1 mm and the clamping pressure was set to 6 bar (60 N cm^{-2}). The measurements were carried out at zero backpressure, at a cell temperature of 70 °C and with gases humidified at 65 °C (Globe Tech inc.). Furthermore, to avoid condensation between the humidifiers and the cell, the temperature of the pipes was set to 77 °C. These conditions were used in all the shut-down strategies, as well as in the electrochemical evaluation.

The gas flow rates were set using mass flow controllers (Brooks Instruments B. V) controlled by LabVIEW software and two NI USB-6008 data acquisition devices (DAQs). The same LabVIEW software was used to control all solenoid valves, and the diaphragm pump used as recirculation pump at the anode. Fig. 1 also shows the solenoid valves between the humidifiers and the cell, which prevents the leakage of gases into the cell from the humidifiers, when required. Furthermore, the solenoid valves at the anode and cathode exhausts prevented the diffusion of air into the cell, when required. An Autolab potentiostat also controlled with the same LabVIEW software was used as load to perform all shut-down strategies. An IM6 unit together with an EL101 Booster (Zahner Elektrik) was used to perform all the electrochemical characterizations, including cyclic voltammetry, H_2 crossover measurements, polarization curves using H_2 at the anode and either O_2 or air at the cathode, and electrochemical impedance spectroscopy (EIS). Table 1 summarizes the operating conditions used for each characterization method.

2.2. Scanning electron microscopy (SEM)

SEM imaging was carried out using a Hitachi S-4800 FE SEM. The analysis of the MEAs cross-sections was obtained by the freeze and break technique described elsewhere [29].

2.3. Shut-down strategies

The shut-down strategies evaluated in this studied are: *i*) *No purge*, *ii*) *Air purge*, *iii*) *H_2 consumption*, *iv*) *O_2 consumption* and *v*) *H_2 purge*. Table 2 summarizes the type and duration of each implemented action during one full cycle. All five strategies began with the same start-up sequence, consisting in the simultaneous introduction of synthetic reformate gas (45% H_2, 23% CO_2 and 32% N_2) into an air filled anode and of air into the cathode (unprotected start-up). This was followed by a 10 s open circuit voltage (OCV) and a 40 s load at a constant current density of 0.5 A cm^{-2}. After the 40 s normal operation the fuel cell is shut-down using one of the above strategies. Finally, all strategies finished their respective cycles with an air purge of both the anode and the cathode, which simulates a prolonged shut-down.

The *No purge* shut-down consisted in not doing anything to either minimize the time or to avoid the H_2/O_2 front at the anode during shut-down. The cell was allowed to reach OCV after the 40 s load at 0.5 A cm^{-2}, the reformate gas and air were shut off and both the anode and cathode exhausts were left opened for at least 820 s. This strategy was only implemented for a total of 230 SU/SD cycles.

The *Air purge* shut-down, a strategy probably used by many fuel cell system developers, consisted in minimizing the time for the H_2/O_2 front at the anode during shut-down. The cell was allowed to reach OCV after the 40 s load at 0.5 A cm^{-2}. Then, the reformate gas was shut off and the solenoid valve between humidifier and anode

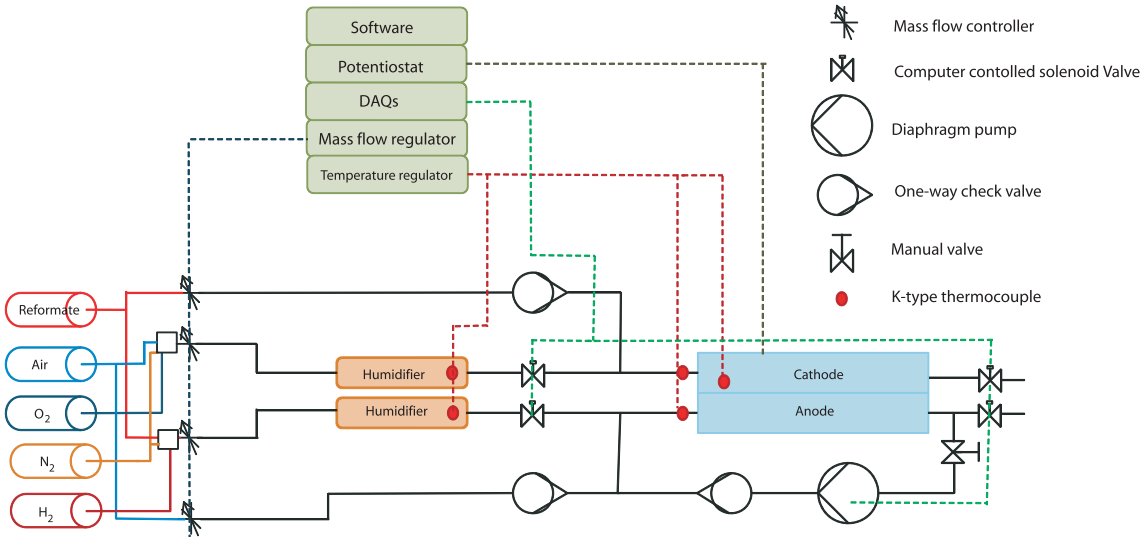

Fig. 1. Illustration of the experimental set-up used to perform the different shut-down strategies.

was closed. The reformate gas from the anode compartment was rapidly removed by purging with 500 ml min^{-1} dry air, while the cathode was continuously supplied with air. This strategy was implemented for a total of 1100 simulated SU/SD cycles.

The *H_2 consumption* shut-down cannot be classified as a common shut-down strategy. It was however selected for evaluation because it provides the opportunity to completely avoid the H_2/O_2 front at the anode during shut-down. Furthermore, this strategy could be one of few shut-down options possible for portable PEMFCs, usually having air-breeding cathodes. After the 40 s load at 0.5 A cm^{-2}, the reformate gas is shut off. The solenoid valve between humidifier and anode, as well as the solenoid valve at the anode exhaust were closed. The diaphragm pump was turned on and the residual reformate at the anode was simultaneously recycled and consumed applying a load program algorithm. The algorithm consisted in applying constant loads of 20, 15, 10, 5, and 1 mA cm^{-2} with a waiting time of 35 s between each current density or until the cell voltage remained below 0.3 V, while the cathode was continuously supplied with air. This strategy was implemented for a total of 1100 simulated SU/SD cycles.

The *O_2 consumption* shut-down, a strategy often encountered in the literature and commonly referred to as shut-down with dummy-load, consisted not only in minimizing the time for the H_2/O_2 front at the anode, but also in protecting the cathode from high potentials during shut-down. After the 40 s load at 0.5 A cm^{-2}, the air is shut off. The solenoid valve between humidifier and cathode, as well as the solenoid valve at the cathode exhaust were closed. A constant load of 50 mA (~7 mA cm^{-2}) was applied until the cell

Table 1
Operating conditions used for the electrochemical characterization of the different shut-down strategies.

Cyclic voltammetry	
Reference electrode gas	H_2
Reference gas flow rate	30 ml min^{-1}
Working electrode gas	N_2
Working gas flow rate	13 ml min^{-1}
Sweep rates	100 and 50 mV s^{-1}
Potential sweep limits cathode CV	0.1–1.2 V vs. RHE
Potential sweep limits anode CV	0.1–0.8 V vs. RHE
Hydrogen crossover measurement	
Reference electrode gas	H_2
Reference gas flow rate	30 ml min^{-1}
Working electrode gas	N_2
Working gas flow rate	60.0 ml min^{-1}
Sweep rate	0.5 mV s^{-1}
Potential sweep limits	0.1–0.7 V vs. RHE
Polarization curves and impedance spectroscopy	
Anode gas	H_2
Anode flow rate	30 ml min^{-1}
Anode stoichiometry	1.2
Cathode gas	O_2 or air
Cathode flow rate	270 ml min^{-1}
Frequency range	100 kHz–100 mHz
Amplitude	10 mV
Current for EIS in O_2 or Air	Same as current density

Table 2
Summarizes the type and duration of each action implemented during each shut-down strategies.

Shut-down strategy	Action	Time
No purge	1. Fuel supply turned on and run cell at OCV	10 s
	2. Run cell at 0.5 A cm^{-2}	40 s
	3. Shut off both fuel and air supply (open exhausts)	820 s
	4. Purge anode and cathode with air	30 s
Air purge	1. Fuel supply turned on and run cell at OCV	10 s
	2. Run cell at 0.5 A cm^{-2}	40 s
	3. OCV	10 s
	4. Purge anode and cathode with air	50 s
H_2 consumption	1. Fuel supply turned on and run cell at OCV	10 s
	2. Run cell at 0.5 A cm^{-2}	40 s
	3. Start pump, shut off fuel supply and run the load program	760 s
	4. Purge anode and cathode with air	30 s
O_2 consumption	1. Fuel supply turned on and run cell at OCV	10 s
	2. Run cell at 0.5 A cm^{-2}	40 s
	3. OCV	5 s
	4. Shut off air supply and run load	100 s
	5. Turn load off and purge anode with dry air	3 s
	6. Purge both anode and cathode with air	30 s
H_2 purge	1. Fuel supply turned on and run cell at OCV	10 s
	2. Run cell at 0.5 A cm^{-2}	40 s
	3 OCV	10 s
	4. Purge cathode with reformate	15 s
	5. Purge anode with air	3 s
	6. Purge anode and cathode with air	30 s

voltage reached 0 V. At this point, the reformate gas was shut off and the solenoid valve between humidifier and anode was closed, and the residual reformate gas from the anode was rapidly removed by purging with 500 ml min^{-1} dry air. This strategy was also implemented for a total of 1100 simulated start-up and shut-down cycles.

Implementation of *H_2 purge* shut-down may not be classified as common and references can only be found in the patent literature [22,23]. This strategy consists in protecting the cathode from high potentials using hydrogen. After the 40 s load at 0.5 A cm^{-2}, the cell was allowed to reach OCV. Then, the air supply to the cathode was shut off, the solenoid valve between humidifier and cathode was closed and the residual air in the cathode was rapidly removed by purging with 500 ml min^{-1} dry reformate gas. Then, the reformate supply to the anode was shut off, the solenoid valve between humidifier and anode was closed, and the remaining reformate gas from the anode was rapidly removed by purging with 500 ml min^{-1} dry air. With only a 3 s delay of the anode air purge, the dry reformate supply to the cathode was turned off, the solenoid between humidifier and cathode was opened and the cathode was purged with 300 ml min^{-1} humidified air, at this stage both the anode and cathode were filled with air. This strategy was also implemented for a total of 1100 simulated SU/SD cycles.

It is important to highlight that the total performance loss for a particular shut-down strategy also includes the performance loss due to unprotected start-ups, as well as the performance loss due to the cycling of the current density (0–0.5 A cm^{-2}). In order to distinguish the SU/SD degradation from the degradation due to this current density cycling, an additional single cell test was carried out. In this test, the current density was cycled between 0 and 0.5 A cm^{-2} (approximately 0.96–0.65 V) for 1100 cycles, with a 20 s OCV between each cycle and without SU/SD.

3. Results

3.1. Cell voltage/current response during shut-down

Fig. 2a–e shows the cell voltage and current density plotted as a function of time for a typical start-up/operation/shut-down cycle for the five different strategies.

Fig. 2a shows the cell voltage/current response of the fuel cell using the *No purge* strategy. The decrease in cell voltage is caused by a relatively slow diffusion of air into the anode compartment, either from crossover through the membrane or from the open anode exhaust. From additional experiments, which are not included in this paper, it was observed that the time needed for the cell voltage to reach 0 V is very dependent on the length of the anode exhaust. Furthermore, the sudden voltage increase and the relatively fast voltage decay observed within the few first seconds of this procedure correspond to an initial anode air purge. This voltage behavior could be related to some back diffusion of H_2 from the fuel cell into the air purge piping. Thus, when the air purge of the anode is initiated, some H_2 may reach the anode, temporarily elevating the cell voltage.

Fig. 2b shows the cell voltage/current response when implementing the *Air purge* shut-down. It shows a fast decrease in cell voltage during the shut-down, indicating that the removal of reformate is accomplished within a few seconds, minimizing the residence time of the H_2/O_2 front.

Fig. 2c shows cell voltage/current response of the *H_2 consumption* strategy. The residual reformate is recirculated and consumed until the cell voltages remained under 0.3 V. The aim is to completely avoiding the H_2/O_2 front at the anode during the final air purge. It is also apparent from Fig. 2c that it takes several hundreds of seconds for the cell voltage to stabilize below 0.3 V. This is due to the low current loads used in an attempt to avoid issues related to fuel starvation. Furthermore, there is a certain degree of concern for possible O_2 crossover from the cathode during this period, which could either react with residual H_2 or create local H_2/O_2 fronts.

Fig. 2d shows the cell voltage/current response of the *O_2 consumption* shut-down in where a low cathode potential is accomplished within 100 s using a small current load (50 mA). The lowering of the cell voltage is assumed not only to be a result of O_2 depletion, but also to the presence of H_2 at the cathode that permeates through the membrane from the anode. It is very important to emphasize that, in contrast to other studies [2,15,24,25], the load is disengaged right before the air purge of the anode ($i = 0$). Otherwise it may have resulted in having ORR at the anode and HOR at the cathode, with possible fuel starvation at the cathode. What is now instead achieved is the OCV between an air-filled Pt-alloy anode and a Pt cathode in the presence of H_2, approximately −0.7 V according to Fig. 2d. This negative cell voltage is only present a few seconds, as the cathode is finally purged with air; however, it creates a certain degree of concern for the Pt-alloy catalyst at the anode. This is because dissolution of the alloy component at higher electrode potentials is well established [30]. Furthermore, the presence of H_2 at the cathode also implies a H_2/O_2 front at the cathode during the final air purge, while having an air filled anode, possibly resulting in carbon corrosion at the anode.

Fig. 2e shows the *H_2 purge* strategy with a fast decrease in cell voltage after normal operation. This indicates that the removal of air from the cathode using reformate gas is accomplished within a few seconds. It is further assumed that this first H_2/O_2 front created at the cathode does not affect the anode, as the anode is protected from high potentials due to the presence of H_2. The same is assumed for the cathode during the air purge of the anode, it is protected from high potentials also due to the presence of H_2. The negative cell voltage (at $i = 0$) experienced by the cell was approximately −0.9 V according to Fig. 2e and is induced during the anode air purge. Analogous to the *O_2 consumption* strategy, the negative cell voltage creates a certain degree of concern for the dissolution of the alloy component from the anode catalyst, as well as possible carbon corrosion at the anode during the final air purge of the cathode. Furthermore, if strategies involving negative cell voltages were to be implemented in real fuel cell applications, the use of a dc–dc converter able to sustain a reversed polarity may be considered.

3.2. Electrochemical characterization

3.2.1. Electrochemically active surface area (ECSA)

Fig. 3a shows the ECSA of the different Pt/C cathodes determined in-situ from the hydrogen desorption peak charge calculated from individual cyclic voltammograms. The charge associated with a monolayer of adsorbed hydrogen on Pt was assumed to be 210 μC cm^{-2} [31]. For comparison the mean value of the ECSA of four fresh cathodes, as well as the ECSA of the cathode submitted to 1100 current density cycles are also plotted in Fig. 3a. The degradation of ECSA due to the current cycling is significant. Approximately 20% of the initial ECSA is lost after 1100 cycles, resulting in a degradation rate of 0.009 m^2 g_{Pt}^{-1} $cycle^{-1}$. Although this value is significant, it is also comparable to values reported in the literature for similar MEAs, cycled under similar conditions [32]. Fig. 3a also shows that the most detrimental for the Pt/C cathode is not implementing a shut-down strategy. The ECSA of the cathode in which the "*No purge*" was used decreases by 80% after only 230 cycles. This dramatic decrease in ECSA has been shown to be typical for corroded cathodes [1,33]. The other four strategies are not only

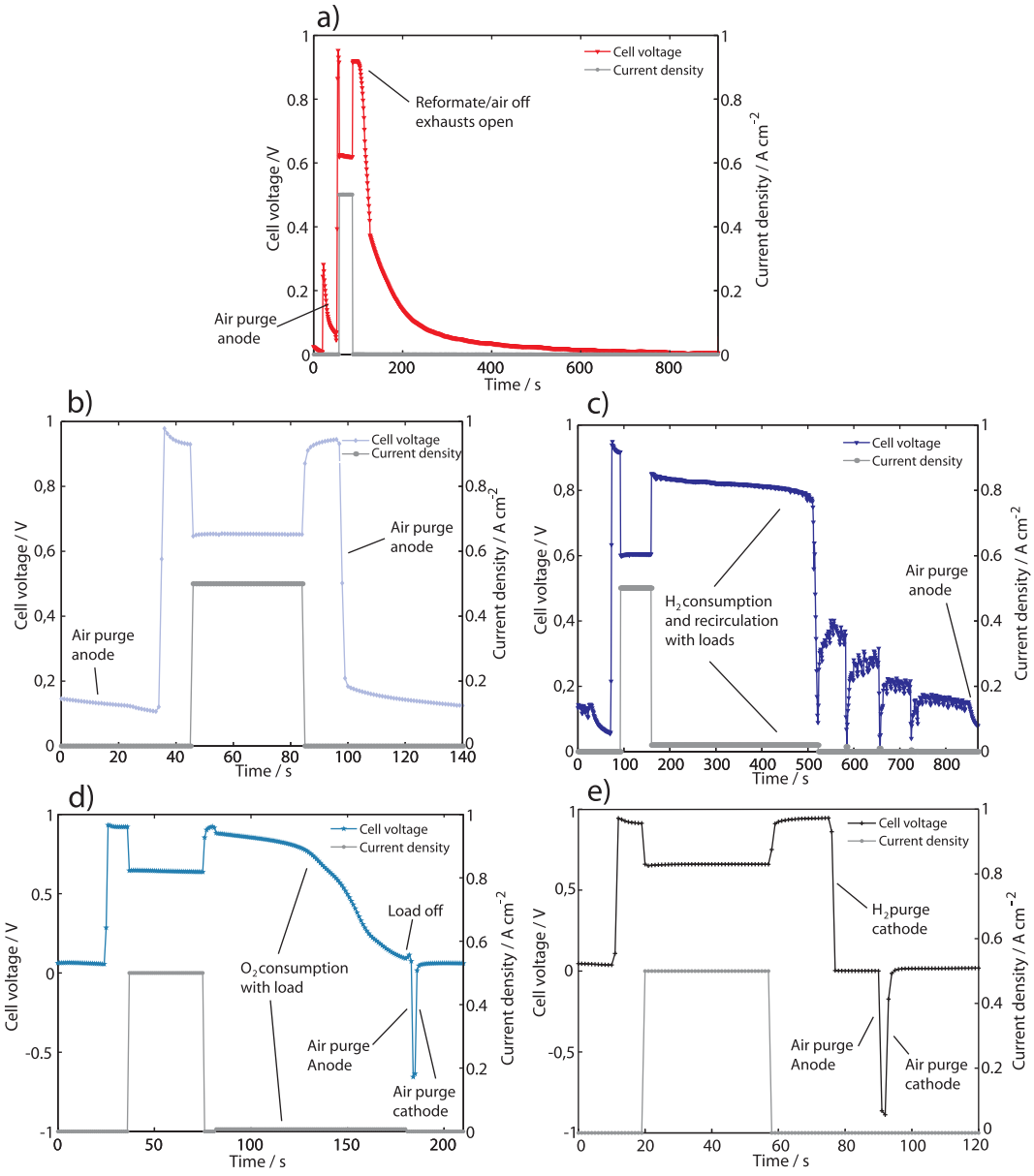

Fig. 2. Cell potential and current density during a typical start-up/operation/shut-down cycle using: a) no purge, b) air purge, c) H_2 consumption, d) O_2 consumption and e) H_2 purge. Conditions: Cell temperature: 70 °C, RH: 80%, fuel: synthetic reformate, oxidant: air.

able to reach 1100 SU/SD cycles, but show much lower ECSA degradation rates. Fig. 3b shows the ECSA degradation rates for the five shut-down strategies, where the ECSA degradation rate corresponding to the current cycling has been subtracted. Thus, the degradation rates corresponding only due to the SU/SD are: 0.158, 0.0216, 0.0242, 0.0131 and 0.0074 $m^2\ g_{Pt}^{-1}\ cycle^{-1}$, for the *No purge*, *Air purge*, *H_2 consumption*, *O_2 consumption* and *H_2 purge*, respectively. From these results it seems as the *O_2 consumption* and *H_2 purge* strategies are able to more efficiently protect the cathode catalyst from degradation. The mechanisms for the decrease in catalyst surface area are not dealt with in this study. However, due to the particular mode of operation of these fuel cells, i.e. cycling the cathode potentials between high and low values, the loss of ECSA is assumed to be caused by a combined effect of Pt dissolution, agglomeration and detachment [34].

Fig. 4 shows cyclic voltammograms performed at the anode of the MEAs subjected to the *O_2 consumption* and *H_2 purge* strategies, in order to identify possible dissolution of the alloy component upon 1100 SU/SD cycles. The voltammogram after 1100 current density cycling is also included for comparison. The anode CVs after 1100 cycles using the *O_2 consumption* and *H_2 purge* strategies show a slight development of a more defined hydrogen adsorption/desorption peaks and showing similar features as to those expected from pure Pt/C CVs. These changes may be due to the loss of the alloy component upon SU/SD using these two particular strategies.

3.2.2. *H_2 crossover*

Fig. 5 shows the H_2 crossover measurements using linear sweep voltammetry (LSV). At 0.5 V vs. RHE, the average crossover current density for fresh MEAs is estimated to be 2.3 ± 0.5 mA cm^{-2}. This large standard deviation imposes some difficulties to visually evaluate the changes in hydrogen permeation rates for the individual MEAs. It is on the other hand possible to state that none of the shut-down strategies showed an increase of the hydrogen

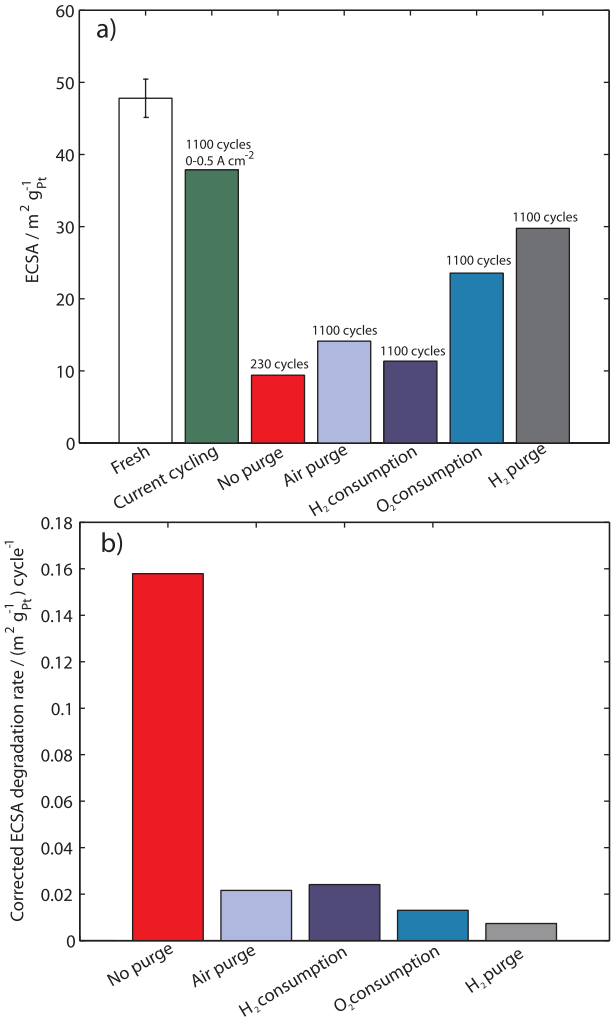

Fig. 3. Electrochemically active surface area (ECSA) calculated from cyclic voltammetry using the hydrogen desorption peak. a) ECSA before and after SU/SD and b) ECSA degradation rate per SU/SD cycle, corrected for the degradation rate due to the current density cycling. Conditions: Cell temperature 70 °C, RH: 80%, gases: H_2 at reference electrode and N_2 at working electrode, sweep rate: 50 mV s^{-1}.

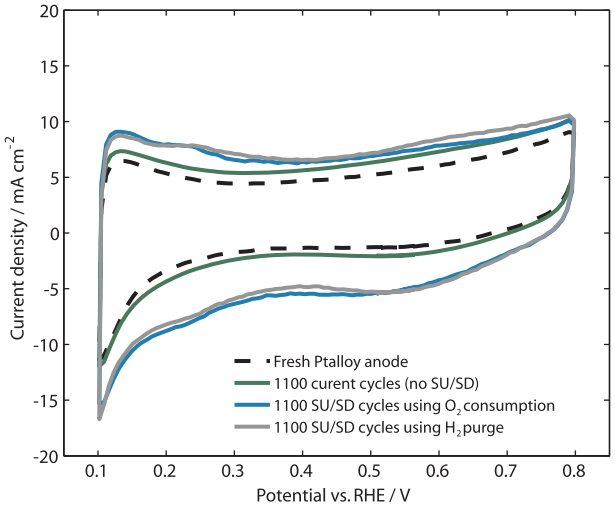

Fig. 4. Cyclic voltammetry of Pt-alloy anodes before and after 1100 SU/SD cycles and after 1100 current density cycles. Conditions: Cell temperature: 70 °C, RH: 80%, gases: H_2 at reference electrode and N_2 at working electrode, sweep rate: 50 mV s^{-1}.

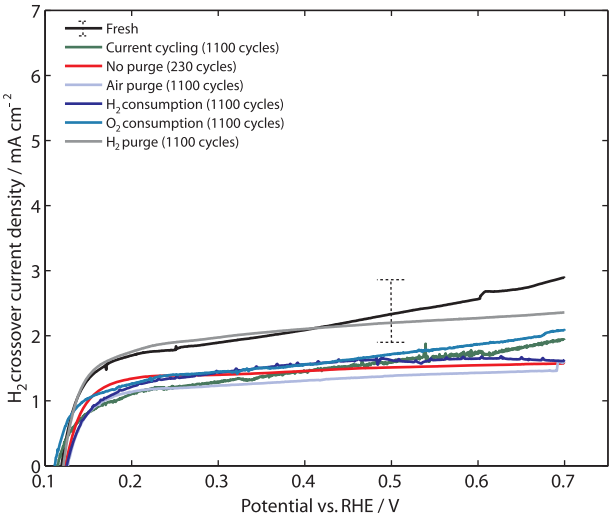

Fig. 5. H_2 crossover measurement using linear sweep voltammetry (LSV). Conditions: Cell temperature: 70 °C, RH: 80%, gases: H_2 at reference electrode and N_2 at working electrode, sweep rate: 0.5 mV s^{-1}.

crossover current density, which is commonly related to pinholes, membrane thinning and general degradation of the membrane.

3.2.3. Specific activity for the ORR

Fig. 6 shows Tafel plots using pure H_2 and O_2 at the anode and cathode respectively. The iR-corrected potential is plotted against $log(i + i_x)$, where i is the measured steady state current density and i_x is the hydrogen crossover current densities. The error bars show an excellent reproducibility between different fresh samples, with a standard deviation of ±4 mV for any given current density. As expected from the ECSA measurements, only the *O_2 consumption* and *H_2 purge* strategies show a sufficiently low decrease in activity for the ORR. In fact, the Tafel plots of these two strategies nearly superimpose the Tafel plot of the current cycling test, with practically no additional degradation. At 0.86 V, the degradation rate of the specific activity due to current cycling is 23 μA cm^{-2} cycle^{-1}. The *No purge*, *Air purge*, *H_2 consumption*, *O_2 consumption* and *H_2 purge* resulted in degradation rates of 282, 57, 62, 28 and 26 μA cm^{-2} cycle^{-1}, respectively. If on the other hand considering the degradation due to current cycling, the degradation rate of the activity due the *O_2 consumption* and the *H_2 purge* may be as low as 5 and 3 μA cm^{-2} cycle^{-1}, respectively.

3.2.4. Ohmic losses

Fig. 7 shows the effect of the shut-down strategy on the resistance of the cell. The resistance was measured at different current densities using EIS, taking the cell resistance value from the real impedance at 2 kHz (HFR). The *No purge* is the only strategy that clearly shows a large increase in HFR (approximately 200 mΩ cm^2 increase) after 230 cycles. The other shut-down strategies also show an increased HFR, which is more visible at low current densities. At 140 mA cm^{-2} the *Air purge*, *H_2 consumption*, *O_2 consumption* and *H_2 purge* strategies cause the HFR to increase from 103 ± 5 mΩ cm^2 to 148, 124, 120, 110 mΩ cm^2, respectively. It is well known that the measured HFR value includes the contribution from several ohmic losses, such as membrane and ionomer resistance, and electrical resistances including contact resistances. Thus, it is difficult to pinpoint the specific ohmic loss causing these changes. It is however proposed that the decreased thickness of the corroded cathode and the possible corrosion of the part of MPL in contact with the electrode [19], may cause the loss of contact between

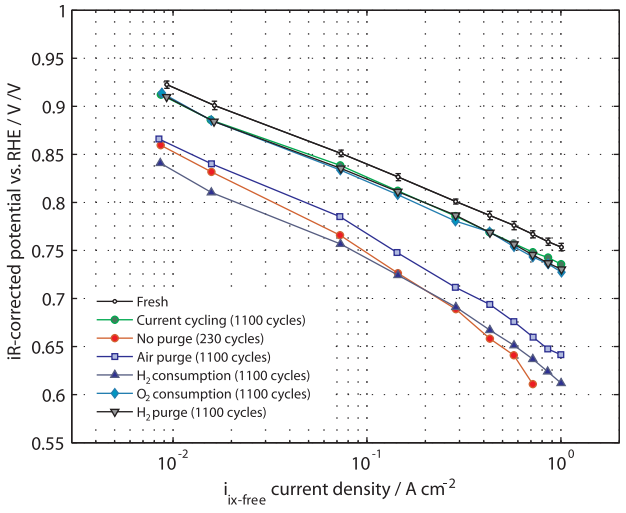

Fig. 6. Tafel plots. Conditions: Cell temperature 70 °C, RH: 80%, gases: pure O_2 and H_2 at the cathode and anode, respectively, The measurements are carried out in galvanostatic mode with an equilibrium time of 5 min at each current density.

electrode and GDL, increasing the contact resistances and the heat production in the cell. Recently, Fairweather et al. [35] measured a dramatic decrease in water retention in cells were the cathode have been corroded. It was suggested that carbon corrosion of the cathode results in higher temperature gradients in the cell, causing the cell to dry out.

3.2.5. Polarization curves in air and O_2-gain

Fuel cells subjected to extensive SU/SD operation usually show the largest degradation at high current densities, where mass transport may be compromised by changes in the electrode morphology. Fig. 8a shows steady state polarization curves for the respective shut-down strategies using H_2 and air at the anode and cathode respectively. Fig. 8a also includes the polarization curves of the current cycling test and fresh MEA for comparison. At 0.86 A cm^{-2}, the cell voltage of a fresh MEA decreases from 565 ± 5 mV to 552 mV after 1100 current density cycles. When correcting for this loss, the degradation rates due to the particular shut-down are estimated to be 183, 229, 49 and 23 μV $cycle^{-1}$, for the *Air purge*, *H_2 consumption*, *O_2 consumption* and *H_2 purge*,

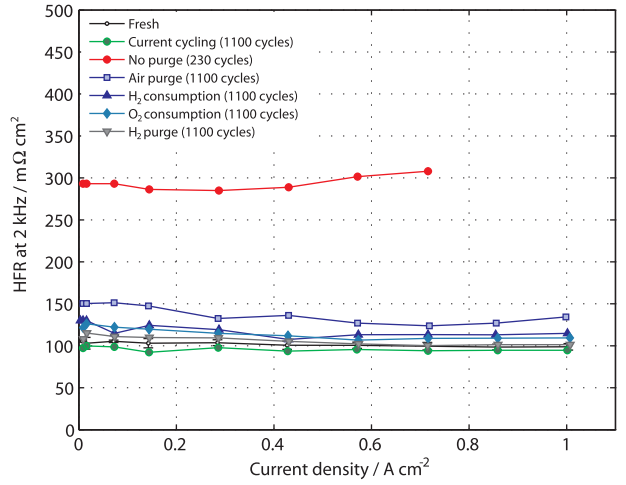

Fig. 7. High frequency resistance (HFR) of the cells. The value is taken from the real impedance (Re(*Z*)) at 2 kHz. Conditions: as in Fig. 6.

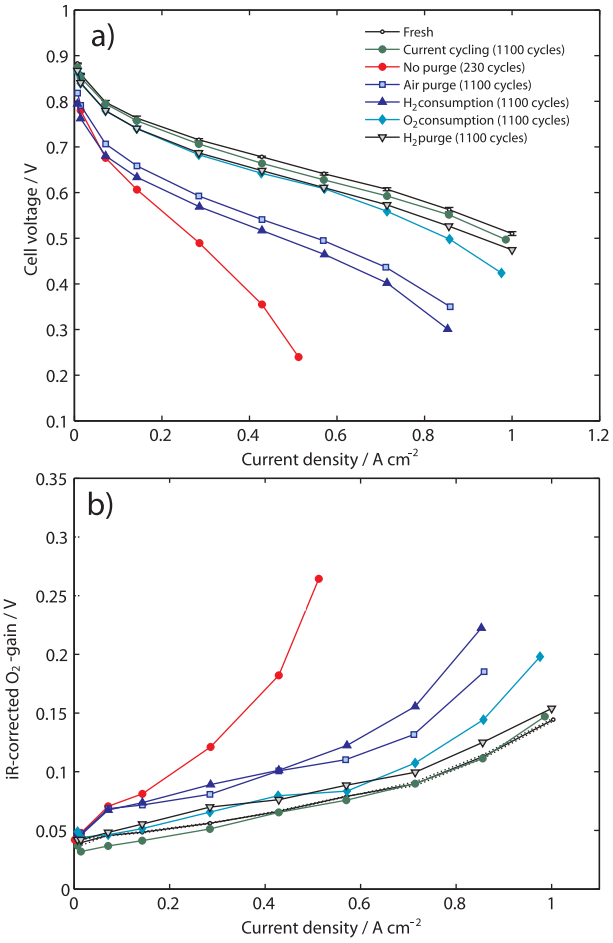

Fig. 8. Polarization curve and O_2-gain. a) Steady-state galvanostatic polarization curve using H_2 and air at the anode and cathode, respectively and b) iR-corrected O_2-gain. Conditions: as in Fig. 6.

respectively. These values are considered to give the best indication on the efficiency of each strategy in protecting the entire MEA, as these values contain activation losses due to loss of Pt surface area, ohmic losses due to membrane and contact resistances, as well as mass transport losses of the electrode and GDL.

To have a clear indication of the mass transport losses, Fig. 8b shows the O_2-gain for the different fuel cells. The magnitude of the O_2 gain is the difference in iR-free cell potential using either pure O_2 or air at the cathode. Thus, the activation losses, as well as the ohmic losses are canceled out and it is therefore a measure of the gas-phase mass transport of the respective cathodes. Already at low current densities (e.g. 100–200 mA cm^{-2}), there is a notable increase of the cathode mass transport losses for the *No purge*, *Air purge* and *H_2 consumption* strategies. This is a clear indication that not only the Pt catalyst has been affected by the type of shut-down strategy, but also the transport properties of the electrode/GDL. Comparing the O_2-gain at high current densities (e.g. 0.86 A cm^{-2}), it is possible to conclude that the *H_2 purge* strategy, is the strategy that has the lowest impact on the mass transport properties of the cathode.

3.2.6. SEM analysis

Fig. 9a–g shows micrographs of the different MEAs cross-sections. The mean thickness of the anode, membrane and cathode was calculated for each MEA from several individual micrographs using the software ImageJ. As seen in Fig. 9a–g, no

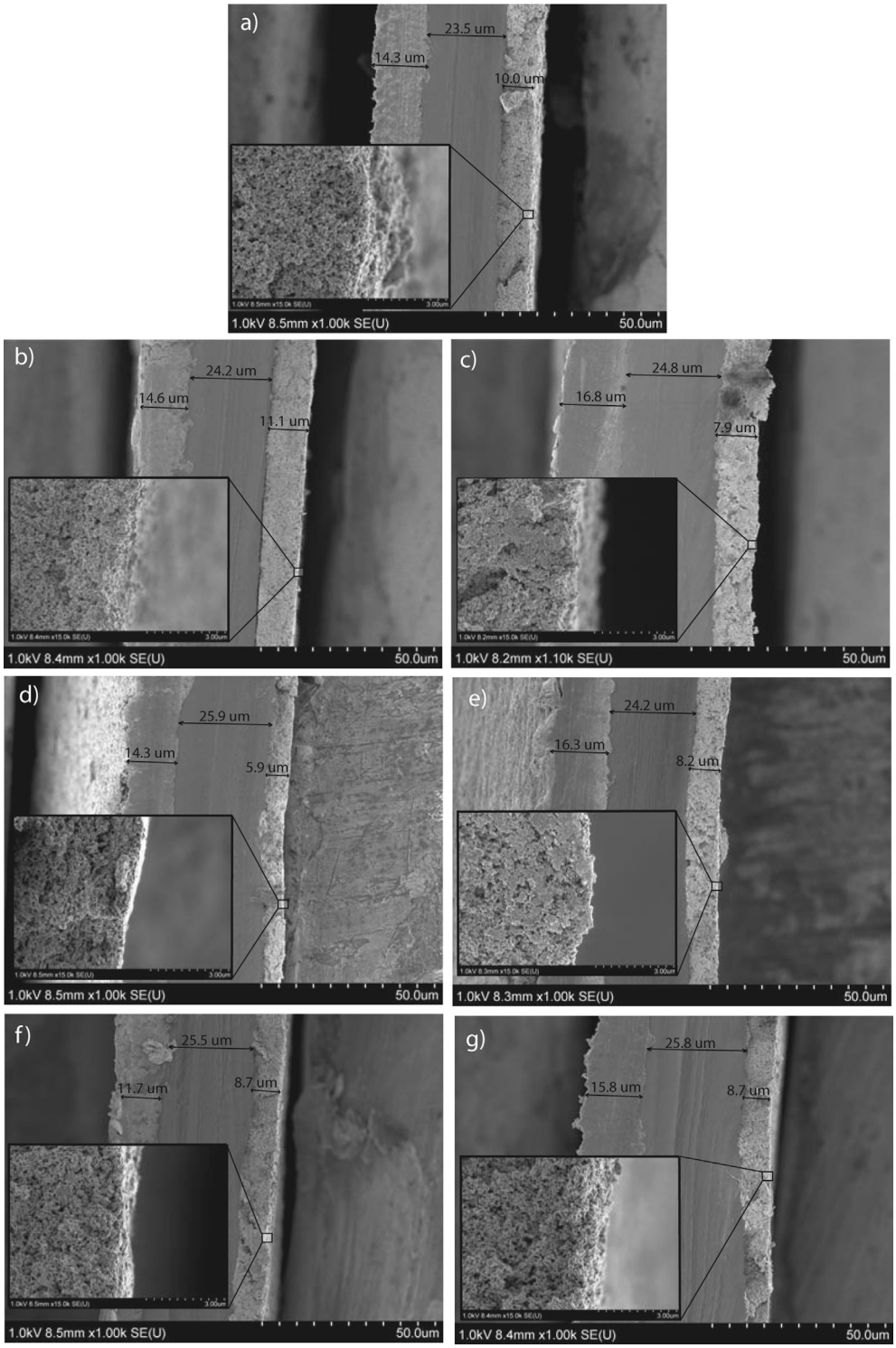

Fig. 9. SEM micrographs of the different MEA cross-sections. a) Fresh, b) current cycling test, c) no purge, d) air purge, e) H_2 consumption, f) O_2 consumption and g) H_2 purge.

considerable changes to the membrane or anode thickness is observed upon repeated SU/SD. The thickness of the membrane is between 23 and 25 μm independent of the shut-down strategy. Furthermore, no pinholes or creeping was possible to observe during the SEM analysis in any of the MEAs. Chemical, mechanical and thermal degradation of the membrane can therefore be considered as negligible. Fig. 9a–g however, reveals some changes to thicknesses of the cathodes. The mean thickness of a *fresh* cathode was estimated to be 10 ± 0.6 μm, and depending on the shut-down decreased to a thickness of 7.9 ± 1.7 μm, 5.9 ± 0.7 μm, 8.2 ± 0.9 μm, 8.7 ± 1.1 μm, and 8.7 ± 0.9 μm for the *No purge*, *Air purge*, *H_2 consumption*, *O_2 consumption* and *H_2 purge*, respectively. Changes to the cathode thickness is probably caused by the loss of carbon from the electrodes due to carbon corrosion, in such case indicating that the *O_2 consumption* and *H_2 purge* shut-downs give better protection against carbon corrosion.

The in-sets of Fig. 9a–g provide a more detailed view of the electrode morphology. The *fresh* cathodes, as well as the cathodes used in the *current cycling* test, *O_2 consumption* and *H_2 purge* strategies show all a narrow pore size distribution with a large amount of visible pores ranging from 40 to 70 nm in diameter, a pore size that is believed to be crucial for proper water management in the electrode. The other shut-down strategies on the other hand, show signs of altered electrode morphology. The cathodes used in the *No purge* and *H_2 consumption* strategies display areas of a total loss of porosity, combined with areas with large cavities >200 nm. For the cathode used in the *Air purge strategy*, areas of total loss of porosity were not clearly observed, however large cavities >200 nm were present.

4. Conclusions

The study compared a few of the most common shut-down strategies for PEMFCs using commercially available components. As known for a number of years, not doing anything to avoid or minimize H_2/O_2 fronts at the anode during shut-downs is detrimental for the fuel cell durability. Consequently, all the applied strategies in this study showed considerably lower degradation rates than the *no purge* strategy. The *Air purge* (183 μV cycle^{-1}) and *H_2 consumption* (229 μV cycle^{-1}) strategies showed relatively high, but comparable degradation rates at 0.86 A cm^{-2} using H_2 and air at the anode and cathode, respectively. The *Air purge* only minimizes the time for the H_2/O_2 front at the anode and therefore only minimized the time for high cathode potentials. The aim of *H_2 consumption* was to completely avoid the H_2/O_2 by consuming the residual H_2 at the cathode. However, it is thought that the crossover of O_2 to the anode may be sufficiently high to cause localized H_2/O_2 regions and therefore carbon corrosion at the cathode [26]. The *O_2 consumption* and *H_2 purge* showed at least one order of magnitude lower degradation rates than the other strategies, 49 and 23 μV cycle^{-1}, respectively. Furthermore, the *H_2 purge* strategy was repeated in order to include measurement errors and resulted in a degradation rate of 21 μV cycle^{-1} at 0.86 A cm^{-2} in H_2/air. With the exception of the results reported by Perry et al. [36] the present degradation rates can be regarded as low, especially considering that these values also include the degradation rate caused by unprotected start-ups having an air-filled anode. In both the *O_2 consumption* and *H_2 purge* strategies, the cathode is protected from high electrode potentials by H_2. In the case of *O_2 consumption*, the hydrogen present at the cathode comes from H_2 crossover, which could result in a cathode only partially protected. In the case of the *H_2 purge*, the protection from high electrode potentials is believed to be more comprehensive, as the H_2 rich gas is directly introduced to the cathode. Another advantage of the *H_2 purge* is that it is simple to implement and could potentially be used during start-ups as well, with no additional components or complex devices as in the case of dummy-loads [37]. On the other hand, the main drawback is the degradation of the anode, especially when using Pt-alloy catalysts. Dissolution of the alloy component was indeed identified by performing cyclic voltammetry on the anode and would certainly affect the performance of a stack using CO containing fuels.

References

[1] C.A. Reiser, L. Bregoli, T.W. Patterson, J.S. Yi, J.D. Yang, M.L. Perry, T.D. Jarvi, Electrochem. Solid-State Lett. 8 (6) (2005) A273–A276.
[2] J.H. Kim, E.A. Cho, J.H. Jang, H.J. Kim, T.-H. Lim, I.-H. Oh, J.J. Ko, S.C. Oh, J. Electrochem. Soc. 156 (8) (2009) B955–B961.
[3] T.W. Patterson, R.M. Darling, Electrochem. Solid-State Lett. 9 (4) (2006) A183–A185.
[4] Y.Y. Jo, E. Cho, J.H. Kim, T.-H. Lim, I.-H. Oh, S.-K. Kim, H.-J. Kim, J.H. Jang, J. Power Sources 196 (2011) 9906–9915.
[5] Y. Ishigami, K. Takada, H. Yano, J. Inukai, M. Uchida, Y. Nagumo, T. Hyakutake, H. Nishide, M. Watanabe, J. Power Sources 196 (2011) 3003–3008.
[6] Z.Y. Liu, B.K. Brady, R.N. Carter, B. Litteer, M. Budinski, J.K. Hyun, D.A. Muller, J. Electrochem. Soc. 155 (10) (2008) B979–B984.
[7] R.N. Carter, B.K. Brady, K. Subramanian, T. Tighe, H.A. Gasteiger, ECS Trans. 11 (1) (2007) 423–433.
[8] E.Y. Rantala, A. Pasanen, P. Kauranen, V. Ruiz, M. Borghei, E. Kauppinen, A. Oyarce, G. Lindbergh, C. Lagergren, M. Darab, S. Sunde, M. Thomassen, S.M. Andersen, E. Skou, Fuel Cells 11 (2011) 715–725.
[9] S.K. Natarajan, J. Hamelin, J. Electrochem. Soc. 156 (2) (2009) B210–B215.
[10] I. Cerri, T. Nagami, J. Davies, C. Mormiche, A. Vecoven, B. Hayden, Int. J. Hydrogen Energy 38 (2013) 640–645.
[11] A. Kongkanand, Z. Liu, I. Dutta, F.T. Wagner, J. Electrochem. Soc. 158 (11) (2011) B1286–B1291.
[12] A.J. Steinbach, K. Noda, M.K. Debe, ECS Trans. 3 (1) (2006) 835–853.
[13] R.T. Atanasoski, L.L. Atanasoska, D.A. Cullen, G.M. Haugen, K.L. More, G.D. Vernstrom, Electrocatalysis (2012) 284–297.
[14] B. Genorio, D. Strmcnik, R. Subbaraman, D. Tripkovic, G. Karapetrov, V.R. Stamenkovic, S. Pejovnik, N.M. Markovic, Nat. Mater. (9) (2010).
[15] J.H. Kim, E.A. Cho, J.H. Jang, H.J. Kim, T.H. Lim, I.H. Oh, J.J. Ko, S.C. Oh, J. Electrochem. Soc. 157 (2010) B104–B112.
[16] U.S. Department of Energy (DOE), Annual Progress Report, Fuel Cells, Catalyst, 2012. http://www.hydrogen.energy.gov/annual_progress.html.
[17] Y. Yu, H. Li, H. Wang, X.-Z. Yuan, G. Wang, M. Pan, J. Power Sources 205 (2012) 10–23.
[18] P. Pei, Q. Chang, T. Tang, Int. J. Hydrogen Energy 33 (2008) 3829–3836.
[19] A.B. Ofstad, J.R. Davey, S. Sunde, R.L. Borup, ECS Trans. 16 (2) (2008) 1301–1311.
[20] C.A. Reiser, D. Yang, R.D. Sawyer, U.S. Patent 6,858,336 B2, 2005.
[21] D. Yang, M.M. Steinbugler, R.D. Sawyer, L.L.V. Dine, C.A. Reiser, U.S. Patent Appl. 0102443 A1, 2002.
[22] C.A. Reiser, D. Yang, R.D. Sawyer, U.S. Patent 6,887,599 B2, 2005.
[23] P.T. Yu, F.T. Wagner, U.S. Patent Appl. 0046106 A1, 2006.
[24] H.-J. Kim, S.J. Lim, J.W. Lee, I.-G. Min, S.-Y. Lee, E.A. Cho, I.-H. Oh, J.H. Lee, S.-C. Oh, T.-W. Lim, T.-H. Lim, J. Power Sources 180 (2008) 814–820.
[25] J.H. Kim, E.A. Cho, J.H. Jang, H.J. Kim, T.-H. Lim, I.-H. Oh, J.J. Ko, S.C. Oh, J. Electrochem. Soc. 157 (1) (2010) B118–B124.
[26] Y. Yu, G. Wanga, Z. Tu, Z. Zhan, M. Pan, Electrochim. Acta 71 (2012) 181–193.
[27] J. Ihonen, F. Jaouen, G. Lindbergh, G. Sundholm, Electrochim. Acta 46 (2001) 2899–2911.
[28] A. Oyarce, N. Holmström, A. Bodén, C. Lagergren, G. Lindbergh, J. Power Sources 231 (2013) 246–255.
[29] A. Lundblad, J. Nippon Med. Sch. 7 (2004) 21–28.
[30] E. Antolini, J. Solid State Electrochem. 15 (2011) 455–472.
[31] J. Bett, K. Kinoshita, K. Routsis, P. Stonehart, J. Catal. 29 (1973) 160.
[32] R. Mukundan, R. Borup, J. Davey, R. Lujan, D. Torraco, F. Garzon, A. Weber, M. Brady, G. James, S. Grot, Annual Progress Report, DOE Hydrogen Program, 2010.
[33] H. Tang, Z. Qi, M. Ramani, J.F. Elter, J. Power Sources 158 (2006) 1306–1312.
[34] R. Borup, J. Meyers, B. Pivovar, Y.S. Kim, R. Mukundan, N. Garland, D. Myers, M. Wilson, F. Garzon, D. Wood, P. Zelenay, K. More, K. Stroh, T. Zawodzinski, J. Boncella, J.E. McGrath, M. Inaba, K. Miyatake, M. Hori, K. Ota, Z. Ogumi, S. Miyata, A. Nishikata, Z. Siroma, Y. Uchimoto, K. Yasuda, K. Kimijima, N. Iwashita, Chem. Rev. 107 (2007) 3904.
[35] J.D. Fairweather, D. Spernjak, A.Z. Weber, D. Harvey, S. Wessel, D.S. Hussey, D.L. Jacobson, K. Artyushkova, R. Mukundan, R.L. Borupa, J. Electrochem. Soc. 160 (9) (2013) F980–F993.
[36] M.L. Perry, T.W. Patterson, C. Reiser, ECS Trans. 3 (1) (2006) 783–795.
[37] T.A. Bekkedahl, L.J. Bregoli, R.D. Breault, E.A. Dykeman, J.P. Meyers, T.W. Patterson, T. Skiba, C. Vargas, D. Yang, J.S. Yi, U.S. Patent 6,913,845 B2, 2005.